



Role of conformational sampling of Ser16 and Thr17-phosphorylated phospholamban in interactions with SERCA

Maryam Sayadi^a, Michael Feig^{a,b,*}

^a Department of Chemistry, Michigan State University, East Lansing, MI, 48824, USA

^b Department of Biochemistry and Molecular Biology, Michigan State University, East Lansing, MI, 48824, USA

ARTICLE INFO

Article history:

Received 8 April 2012

Received in revised form 18 August 2012

Accepted 21 August 2012

Available online 29 August 2012

Keywords:

SERCA

Calcium pump

Implicit membrane

Heterogeneous dielectric

Molecular dynamics

Replica exchange

ABSTRACT

Phosphorylation of phospholamban (PLB) at Ser16 and/or Thr17 is believed to release its inhibitory effect on sarcoplasmic reticulum calcium ATPase. Ser16 phosphorylation of PLB has been suggested to cause a conformational change that alters the interaction between the enzyme and protein. Using computer simulations, the conformational sampling of Ser16 phosphorylated PLB in implicit membrane environment is compared here with the unphosphorylated PLB system to investigate these conformational changes. The results suggest that conformational changes in the cytoplasmic domain of PLB upon phosphorylation at Ser16 increase the likelihood of unfavorable interactions with SERCA in the E2 state prompting a conformational switch of SERCA from E2 to E1. Phosphorylation of PLB at Thr17 on the other hand does not appear to affect interactions with SERCA significantly suggesting that the mechanism of releasing the inhibitory effect is different between Thr17 phosphorylated and Ser16 phosphorylated PLB.

© 2012 Elsevier B.V. All rights reserved.

1. Introduction

Phospholamban (PLB), a 52 residue transmembrane (TM) protein, plays an essential role in regulating sarco-/endoplasmic reticulum calcium ATPase (SERCA), a calcium pump in heart muscle [1] by reducing the enzyme affinity for calcium [2]. PLB can be phosphorylated at Ser16 and/or Thr17 by cAMP-dependent protein kinase A (PKA) and Ca²⁺-calmodulin dependent protein kinase (CAM kinase), respectively, in response to β -adrenergic stimulation [3]. PLB phosphorylation increases the Ca²⁺ affinity of SERCA and releases the inhibitory effect [4]. Several *in vivo* studies have shown that phosphorylation of Ser16 and Thr17 is sequential [5,6]. *In vitro* studies in sarcoplasmic reticulum (SR) membranes on the other hand have shown that Thr17 phosphorylation can be stimulated by electrical pulse without the prerequisite of Ser16 phosphorylation [7–9]. It has been suggested that the sequential phosphorylation *in vivo* is a result of interactions between PKA and CaMKII pathways [10]. Ser16 phosphorylation of PLB appears to be sufficient to release the inhibitory effect for the maximum cardiac response to β -adrenergic stimulation [11]. Therefore, the physiological role of Thr17 phosphorylation is not fully understood yet. Interestingly, aerobic interval training preferentially increases Thr17 phosphorylation [12]. It has been suggested that Thr17 and Ser16 phosphorylation may have an

additive effect in releasing the inhibitory function of PLB both *in vitro* [13,14] and *in vivo* [15]. The possibly different physiological role of Ser16 vs. Thr17 phosphorylation may also point at mechanistic differences in SERCA–PLB interactions with PLB phosphorylation at either site.

To better understand the mechanism by which Ser16 and/or Thr17 phosphorylation relieves inhibition of SERCA by PLB, detailed knowledge of the structural changes of PLB upon phosphorylation is essential. Most experimental and computational studies have been focused on unphosphorylated PLB and relatively little detailed structural information is available for phosphorylated PLB. NMR studies of unphosphorylated PLB in DPC micelles [16] and lipid membranes [17,18] suggest an ensemble of L-shaped structures where a long TM helix is connected to a dynamic cytoplasmic (CP) helix via a flexible linker. Based on NMR data, average interhelical angle of $80 \pm 20^\circ$ has been reported in different solutions [19], micellar and membrane environments [16,18], while other experimental data indicate that the CP domain of PLB is in fact in equilibrium between dynamically ordered and disordered conformations [20,21]. The average structural properties and conformational dynamics of PLB have been reproduced by molecular dynamics (MD) simulations from our group [22] and others [23–27].

Phosphorylation of PLB appears to shift the equilibrium of the cytoplasmic helix towards a “disordered” state [28,29], although the exact molecular interpretation of this finding is unclear. Furthermore, a reduction of helical content in the CP helix upon Ser16 phosphorylation has been suggested from CD [30], NMR [31] and attenuated total reflection FTIR (ATR-FTIR) experiments [32]. NMR studies on a

* Corresponding author at: Department of Biochemistry and Molecular Biology, Michigan State University, East Lansing, MI, 48824, USA. Tel.: +1 517 432 7439.

E-mail address: feig@msu.edu (M. Feig).

36-residue long N-terminal fragment of Ser16 and Thr17 phosphorylated PLB also report a shorter CP helix from residues 2 to 12 [33], while the interhelical angle in double phosphorylated PLB appears to be increased to $100 \pm 35^\circ$ [33]. Results from fluorescence resonance energy transfer (FRET) studies indicate a reduced interdomain distance between residues Tyr6 and Cys24 after Ser16 phosphorylation [34]. This is consistent with fluorescence quenching studies of Tyr6, suggesting that phosphorylation reduces the solvent accessibility of Tyr6 as a result of a conformational change [35].

Several experimental studies are consistent with the idea that PLB is still attached to SERCA after phosphorylation [29,34,36–39]. On the other hand, an earlier cross-link study reported the abolishment of cross-links between SERCA and PLB upon phosphorylation by PKA [40], which was interpreted as complete dissociation of PLB from SERCA. However, a more recent cross-link study is more consistent with the data supporting the hypothesis that PLB does not dissociate from SERCA upon phosphorylation [41]. In that study, phosphorylation of PLB on Ser16 increased the distances between certain residues of PLB and SERCA while other cross-links remained the same [41]. An early EPR study also suggests the complete dissociation of PLB from SERCA [42]. There, the shift to the pentameric state of PLB upon phosphorylation was observed in the pentamer–monomer PLB equilibrium. This shift was interpreted as an evidence for dissociation of PLB from SERCA, which binds to the monomeric state of PLB [42]. Finally, fluorescence measurements of PLB–SERCA co-crystals have suggested an alternative hypothesis that phosphorylation of PLB may relieve the inhibitory effect by facilitating the structural coupling between two interacting SERCA units that is otherwise disrupted by unphosphorylated PLB [43].

A few MD simulations of phosphorylated PLB (pPLB) have been reported to date and resulted in the following findings. A decrease in helicity was observed upon Ser16 phosphorylation in simulations of the cytoplasmic PLB domain (residues 1–25) [24]. MD simulations of full length pPLB in an explicit POPC membrane bilayer also showed a decrease in the helical content while interactions of phosphoserine with the membrane head group region appeared to result in lower mobility of the CP domain [27]. Another MD simulation study using both replica exchange simulations of the CP domain of PLB and a constant temperature MD simulation of full-length pPLB has provided further insights. The results from this study suggest a decrease in the interdomain distance, a decreased interhelical angle, and again a loss of helical contents in the CP helix upon phosphorylation as a result of interactions between the Ser16 phosphate group and residues Arg9, Arg13 and/or Arg14 [25]. These simulations of pPLB provide important insight into the structure and dynamics of PLB upon phosphorylation but the covered time scales remain relatively short compared to the experimentally observed dynamics, reaching at best tens of nanoseconds in the replica exchange runs.

In order to describe the dynamics of phosphorylated PLB over much longer time scales, we are reporting here results from replica exchange implicit membrane simulations of PLB that is phosphorylated either at Ser16 or at Thr17. We used here the HDGB implicit membrane model that has been successfully applied in previous simulations of unphosphorylated PLB [22], influenza fusion peptide [44], and integral membrane proteins [45]. An implicit description of the membrane and solvent drastically accelerates sampling because lipid relaxation processes are avoided. We estimate that the combination of using the implicit membrane model with replica exchange sampling provides access to dynamics that would otherwise be observed on microsecond to millisecond time scales. The drawback of using an implicit approach is of course the neglect of explicit lipid-peptide interactions; however, previous studies from our group suggest that the HDGB model used here is able to capture the structure and dynamics of membrane-bound peptides, including PLB, in a highly realistic fashion [22,44].

In the following, the methods used here are briefly summarized before the results are presented and discussed.

2. Methods

2.1. Simulations

Replica exchange MD simulations [46] of monomeric PLB phosphorylated at Ser16 (p16-PLB) or Thr17 (p17-PLB) were carried out and compared with a previous simulation of unphosphorylated PLB [22]. Model 1 of the NMR ensemble for the C36A/C41F/C46A PLB mutant (PDB ID: 1N7L [16]) was used as the initial structure. Zwitterionic termini and standard protonation states (pH = 7) were applied. The phosphoserine and phosphothreonine side chains were assumed to be fully deprotonated with a -2 charge. Starting conformations were oriented in the implicit membrane with the transmembrane (TM) helix parallel to the membrane normal and the cytoplasmic (CP) helix above and parallel to the membrane surface. The CHARMM22 all-atom force-field [47] along with the CMAP correction term [48] was used to describe the peptide interactions. No cutoffs were applied to the non-bonded interactions. The implicit description of the membrane involved the heterogeneous dielectric generalized Born model (HDGB) [49]. Optimized parameters for DPPC bilayer [22] were used in all simulations. Other implicit solvent parameters were set as described previously [50]. The SHAKE algorithm [51] was applied to constrain bonds involving hydrogen atoms. To control the temperature, Langevin dynamics [52] was used with a friction coefficient of 10 ps^{-1} applied to heavy atoms [53]. A time step of 1.5 fs was used to maintain stable simulations with the implicit membrane model as described previously [54]. All simulations were carried out with version 34a2 of CHARMM [55] in combination with the MMTSB Tool Set [56].

Replica exchange simulations consisted of eight replicas over a temperature range of 300–400 K, spaced exponentially. All of the replicas were started with energy-minimized structures. Exchanges were attempted after every 500 MD steps (0.75 ps). The resulting exchange acceptance ratio was 21–30% between adjacent replicas. Four separate replica exchange simulations were carried out for each system and sampling data were combined to improve statistical significance [22]. Each simulation was carried out for 50,000 cycles (37.5 ns/replica)

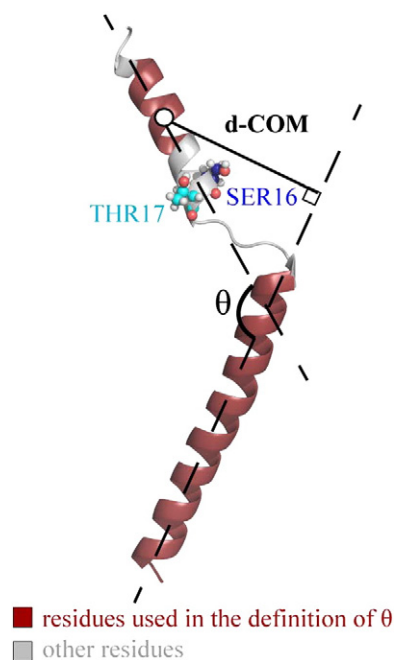


Fig. 1. Reaction coordinates used in generating the PMF plots; interhelical angle, θ , and the distance between the center of mass of the CP helix from its projection onto the TM helical axis, d-COM. Shorter CP helical domain that is used to define θ is colored differently as well as the TM domain.

from which the first 20,000 cycles were considered as equilibration and not included in the analysis. The total length of the production runs is 67.5 ns (22.5 ns for each simulation) for the non-phosphorylated PLB and 90 ns for the p16 and p17 phosphorylated PLB systems (22.5 ns for each simulation).

The weighted histogram analysis method (WHAM) [57] was used to generate potentials of mean force (PMFs) at 300 K to include sampling data at higher temperatures as well. The interhelical angle and the distance between the center of mass of the CP helix and its projection onto the TM helix (d_{COM}) were chosen as the primary reaction coordinates for generating the PMFs (see Fig. 1). The interhelical angle (θ) is defined as the angle between the CP (residues 4–12) and TM (residues 23–52) helical axis. The center of mass of the CP helix was calculated based on residues 1 to 16. Note that the definitions of the reaction coordinates here are slightly different from our previous definition [22] to better describe conformations with less well-defined helical structure. Further analysis involved clustering with the K-means method as implemented in the MMTSB Tool Set [56]. PyMOL was used to generate molecular graphics [58]. MATLAB

version 7.9.0.529 (R2009b) was used to generate PMFs and for data mining analysis.

2.2. SERCA-PLB docking

In order to test whether different PLB conformations are likely to interact favorably with SERCA the following procedure was applied. The TM domain of PLB composed of residues 21–52 (called T-PLB) from the NMR structure (PDB ID: 1N7L) was manually docked to the structure of SERCA in the E2 conformation (PDB ID: 1IWO [59]). To obtain the docked complex, cross-linking information according to Table S1 was used [60–63]. The final distances in the resulting SERCA-PLB complex were close to the cross-linking distances (see Table S1). TM domain of all different conformations of PLB and phosphorylated PLB were then aligned to the docked T-PLB. From all of the aligned PLB structures, residues 1–22 (called cpPLB) were selected and added to the PDB structure of SERCA in the E2 conformation. The complexes were minimized for only 100 steps to correct any possible clashes between the side chains of the two proteins. In order to

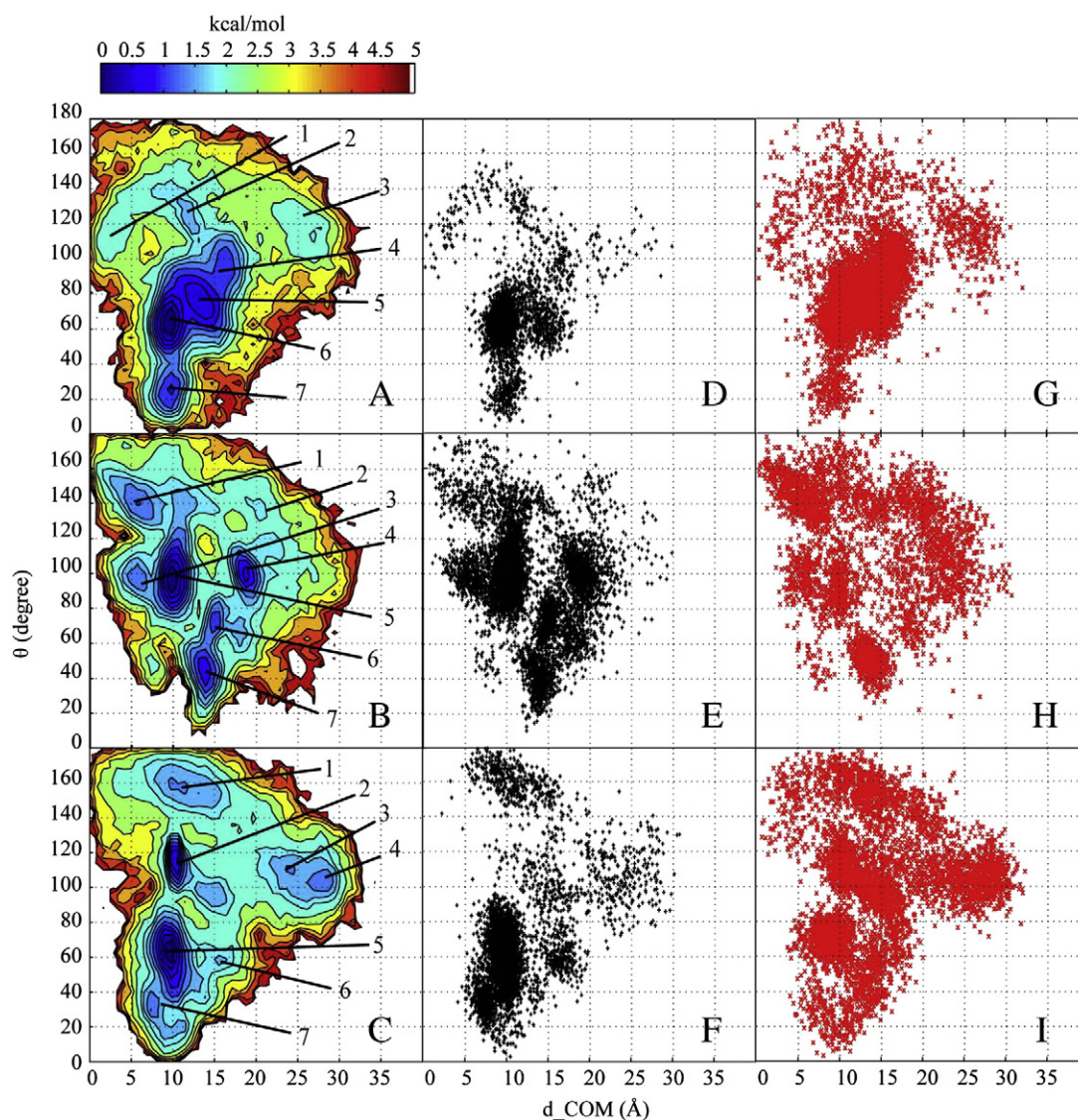


Fig. 2. PMFs as a function of θ and d_{COM} (see Fig. 1), for (A) PLB, (B) p16-PLB, (C) p17-PLB. Representative structures from cluster analysis that correspond to minima are shown. Mapping structures with (shown with \times) and without clash (shown with $+$) in the θ and d_{COM} coordination space for (D, G) PLB, (E, H) p16-PLB, and (F, I) p17-PLB. Conformations sterically incompatible with complex formation are shown in the middle column in black, compatible conformations are shown in red in the right column.

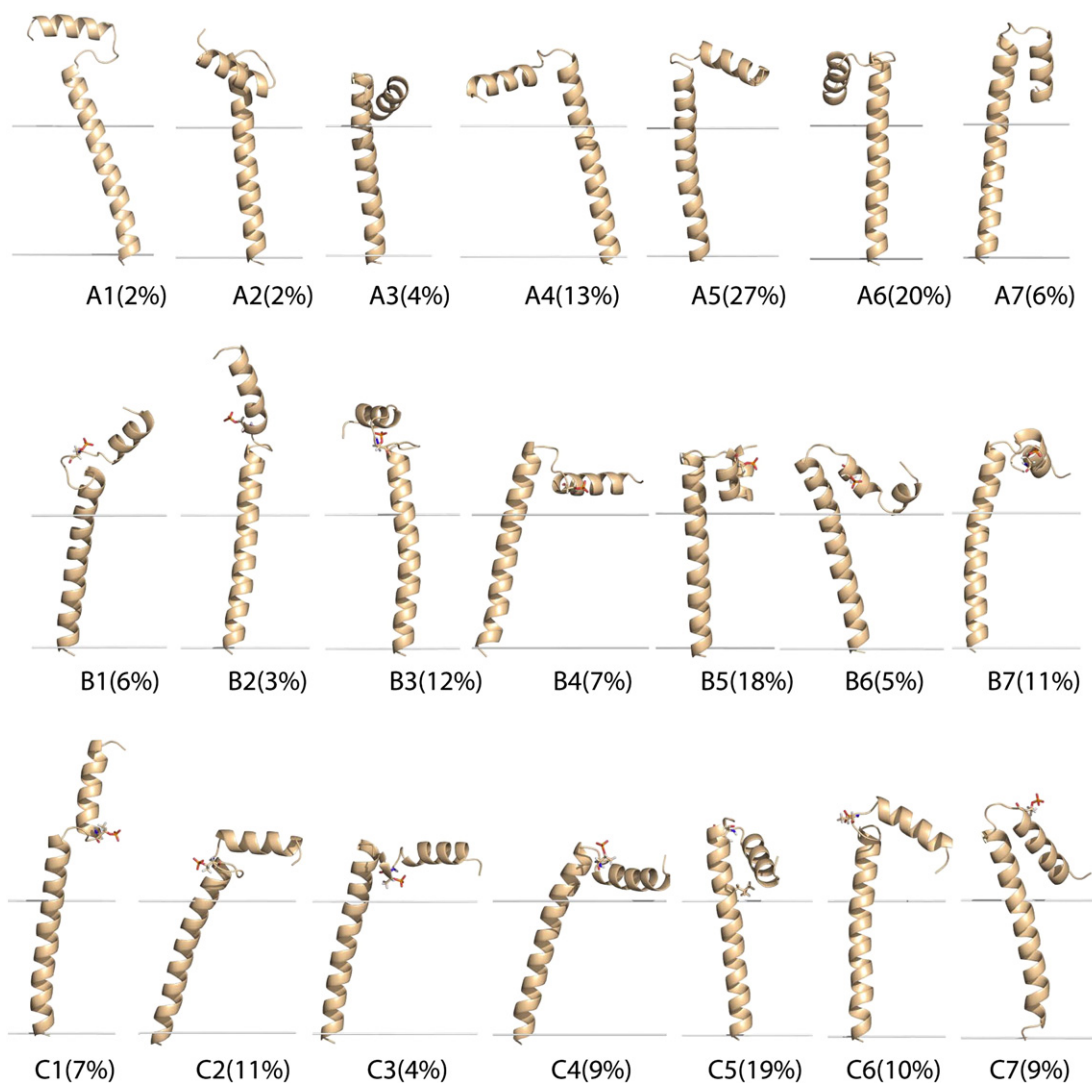


Fig. 3. Representative structures from cluster analysis for (A1-7) PLB, (B1-7) p16-PLB, and (C1-7) p17-PLB that correspond to minima on Fig. 2A–C. In all structures, the orientation with respect to the membrane was preserved. Lines represent the membrane hydrophobic core and are placed at 15 Å distance above and below the membrane center ($z=0$). Ser16 in B1-7 and Thr17 in C1-7 are shown with stick representation. Cluster population percentages are given in parentheses.

obtain a docking score, minimized structures of the complexes were then reduced to a coarse-grained (CG) model with a single site per residue. The CG model was used to focus on the overall shape compatibility and avoid excessive sensitivity to individual atomic contacts that could be relieved through side chain reorientation. The TM

domain of PLB in all of the structures is well-preserved in the simulations. Therefore, only the CP domain of PLB is included in the complexes and calculation of the docking score. Each CG particle is placed at the average position of all the atoms in a given residue.

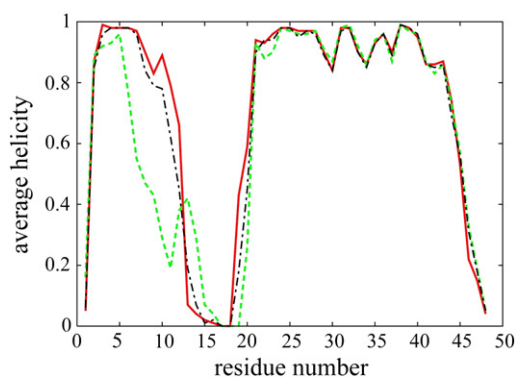


Fig. 4. Average helicity distribution for different residues for PLB (—), p16-PLB (---) and p17-PLB (-.-.-).

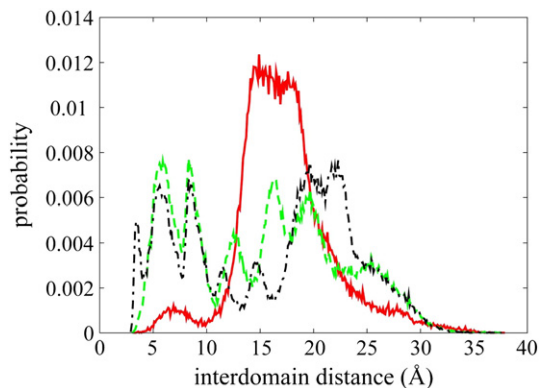


Fig. 5. Distribution of the interdomain distance between the oxygen atom of the hydroxyl group on Tyr6 and the C β atom of Ala24 for PLB (—), p16-PLB (---), and p17-PLB (-.-.-).

Table 1

Comparison between the calculated properties from the simulation and experimental values for the PLB and phosphorylated PLB systems. Uncertainties are obtained from comparing values between different simulations. Standard deviations are given in parentheses.

	Simulation			Experiment	
	PLB	p16-PLB	p17-PLB	PLB	p16-PLB
Interhelical angle ($^{\circ}$) ^a	77.4 ± 7.1 (26.8)	98.0 ± 8.2 (31.0)	89.7 ± 6.2 (36.4)	~80 ± 20 [16–19] ~66 [18]	N/A
Interdomain distance (\AA) ^b	17.3 ± 1.0 (4.4)	15.3 ± 2.6 (7.1)	17.9 ± 1.2 (7.5)	21.1 ± 0.9 [34]	18.2 ± 0.6 [34]
Solvent exposed area of Tyr6 (\AA^2)	139.9 ± 2.3 (21.6)	66.4 ± 30.1 (54.2)	129.5 ± 4.6 (35.6)	31% Decrease upon phosphorylation [35]	

^a Angle between the CP and TM helical vectors.

^b Distance between Ala24 C β and the Tyr6 hydroxyl oxygen.

Only Lennard–Jones interactions were considered in the docking score with the parameters reported in Table S2. Energies were then calculated for the CG models of the SERCA–cpPLB complexes to determine whether CP domain of PLB structures clash with SERCA or not. An energy cutoff of 20 kcal/mol was found to roughly match a more subjective analysis based on visual inspection. Following this protocol, the structural ensembles from the simulations were evaluated to determine the fraction of conformations that are likely to interact favorably with SERCA.

3. Results

Replica exchange simulations of phosphorylated PLB are compared here with previous simulations of unphosphorylated PLB [13]. In order to characterize the dynamics of the cytoplasmic (CP) helix, the simulation data were first analyzed in terms of the angle between the TM and CP helices, θ , and the distance of the center of mass of the CP helix from its projection on the TM helical axis, d-COM (see Methods section for detailed definitions). The resulting PMFs and representative structures corresponding to the minima are shown in Figs. 2A–C and 3, respectively. A wide range of structures was sampled with either of the two phosphorylation states. Generally, the ensembles include compact structures, where the CP helix interacts with the membrane interface, and extended structures, where the CP helix points away from the membrane. Compact structures include L- and T-shaped states with θ values between 50 and 90° as well as conformations with small values of θ of less than 30°, where the CP helix is packed in an antiparallel fashion against the TM helix.

In unphosphorylated PLB, most of the sampling involves L- and T-shaped structures with a small additional population of extended states (see Figs. 2A and 3). Upon phosphorylation at Ser16, additional local minima regions appear in the free energy landscapes. The most

dominant structures are still L- and T-shaped states (cf. B3, B4, and B5 in Fig. 3) with the L-shaped structures more populated relative to the unphosphorylated state. Looking at Fig. 3 it can be seen that structures in the most populated cluster B5 as well as in B6 have a break in the CP domain. These structures are not observed in unphosphorylated PLB and are apparently stabilized by extra hydrogen bonds that involve the phosphorylated Ser16. On the other hand, structures with small θ values below 30° are less populated and structures with $\theta < 10^{\circ}$ are absent altogether in the Ser16 phosphorylated PLB ensemble. This can also be explained by extra hydrogen bonds formed in the CP domain. These extra hydrogen bonds cause the CP helix to break and the N-terminal part comes upward and points away from the membrane center instead of inserting deeply into the membrane. Reduced helicity in the CP helix upon Ser16 phosphorylation is also apparent in the other structures shown in Fig. 3 (cf. B3 and B7). Thr17 phosphorylation, on the other hand, leads to an ensemble that is more similar to unphosphorylated PLB. However, there is more significant sampling of extended structures ($\theta > 150^{\circ}$) as well as structures with small d-COM values (like B4) appear to be less prominent upon Thr17 phosphorylation (see Fig. 2), while highly extended conformations and completely L-shaped conformations such as C1 and C4 in Fig. 3 are sampled more extensively.

To understand the effect of phosphorylation further, a number of other structural properties were analyzed. First, the average helicity was calculated as a function of residue number. The results, presented in Fig. 4, show that phosphorylation at Ser16 significantly reduces the helicity in the CP domain of PLB. This is in agreement with the experimental data [31,32] and confirms results from previous simulation studies [24,27,46]. NMR studies of the PLB (1–25) peptide suggest that residues 12 through 17 unwind upon phosphorylation at Ser16 [30]. According to NMR studies of the full-length monomeric PLB, residues 14 through 17 from the C terminus and residue 3 from the N terminus of the CP helix in the Ia domain of PLB unfold upon phosphorylation at Ser16 [28]. As it is shown in Fig. 4, on average, residues 7 through 11 from the CP helix lose their high helical content upon phosphorylation at Ser16. The number of residues that lose their helical property is more than what is suggested by NMR study of the full-length PLB [28] but is in good agreement with the NMR study of the PLB (1–25) peptide [30]. The helical content of the Ib domain is not influenced by the Ser16 phosphorylation of PLB in agreement with the NMR data [28]. Interestingly, phosphorylation at Thr17 does not appear to affect helicity compared to the unphosphorylated PLB.

Second, interdomain distances between the oxygen atom of the hydroxyl group on Tyr6 and the C β atom of Ala24 were calculated

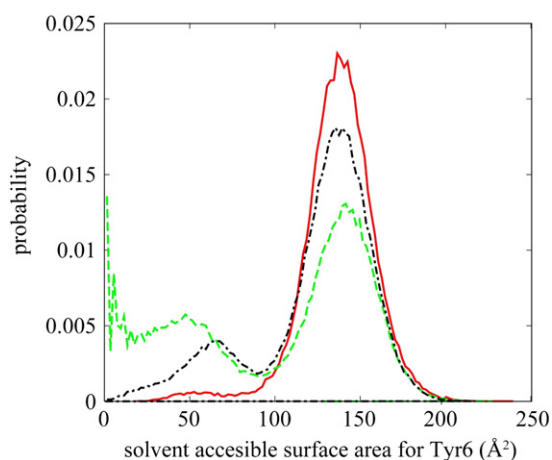


Fig. 6. Distribution of Tyr6 solvent accessible surface area for PLB (—), p16-PLB (---), and p17-PLB (-.-.-).

Table 2

Predicted percentage of PLB structures that clash with SERCA in the E2 state as a function of phosphorylation.

Phosphorylation	None	Ser16	Thr17
Percentage of structures that clash with SERCA	38	69	48

(see Fig. 5). The corresponding distance distributions differ significantly as a function of the phosphorylation state. In its unphosphorylated state, PLB exhibits interdomain distances that lie mostly between 12 and 22 Å. Upon phosphorylation, a diverse set of structures gives rise to a much broader distribution with distances between 3 and 30 Å. Phosphorylation at Thr17 results in a slightly wider interdomain distances relative to Ser16 phosphorylated conformations. FRET experiments have suggested that phosphorylation of PLB at Ser16 decreases the interdomain distance by 3 Å [34]. From the simulations, we found a 2 Å decrease in the overall average interdomain distance, which is considered to be in excellent agreement with experimental data (see Table 1) considering the uncertainties in interpreting the FRET data when sampling of multiple conformations with a wide distribution of distances is involved.

The solvent accessibility of Tyr6 was further analyzed by calculating its solvent accessible surface area (SASA). We found that phosphorylation at Ser16 increases sampling of conformations where Tyr6 is partially or completely buried. In unphosphorylated PLB, Tyr6 is solvent-exposed in almost all of the structures (see Fig. 6). The average solvent-accessible surface area (see Table 1) is reduced by 52% upon Ser16 phosphorylation, but the margin of error is relatively large. This result agrees at least qualitatively with the 31% decrease in the solvent-accessibility measured by fluorescence studies [35].

Finally, the key question is how the conformational changes in PLB upon phosphorylation affect interactions with SERCA and how Ca^{2+} flux is consequently regulated by PLB. While full experimental structures of SERCA–PLB complexes are not available so far, EPR data suggest that by binding to SERCA, the equilibrium between the R and T states of PLB shifts toward the R state without introducing new conformational states for PLB [38]. Under the assumption that PLB in the PLB–SERCA complex resembles conformations seen also in the monomeric form, we performed docking of the PLB structures sampled in our simulations (in the absence of SERCA) to the inactive E2 conformation of SERCA. This was achieved by docking the TM helix of PLB into SERCA according to the cross-linking data first and then, superimposing each of the sampled PLB structures at the TM helix region (see Methods section for more details). We then analyzed the clashes between the CP helix of PLB and SERCA to determine whether the complex was viable. The results of this analysis are given in Table 2. It is found that about 60% of the conformations of unphosphorylated PLB but only 31% of the conformations of Ser16-phosphorylated sampled in the absence of SERCA are structurally compatible with complex formation. We note, that the quality of the intermolecular interactions plays an additional role in determining SERCA–PLB interactions. However, without reliable structural information, such an analysis is likely not meaningful and was therefore not carried out here. Based on the differences in the amount of steric clashes, the simulation results predict that Ser16 phosphorylation would have a destabilizing effect on the PLB–SERCA–E2 complex and likely require a conformational rearrangement of PLB with respect to SERCA if Ser16 phosphorylated PLB stays bound to SERCA as suggested by experiments [29,34,36–38]. Presumably, such a change would allow SERCA to switch from E2 to the active E1 form. Interestingly, Thr17 phosphorylation seems to have a different effect. About half of the conformations sampled in the simulation are still compatible with complex formation. Therefore, at least the interaction of the PLB's CP helix with SERCA may not be completely different from the unphosphorylated complex.

To understand the conformational characteristics of the structures that clash with SERCA better, the sampled conformations were divided into two groups based on whether they clash with SERCA or not. In Fig. 2D–I all these structures have been projected onto θ and d-COM for the PLB and phosphorylated PLB ensembles. Comparing Fig. 2E, F, H, and I shows that even though most of the L- and T-shaped conformation with θ values between 60 and 100° potentially clash with SERCA in the Ser16 phosphorylated state, L- and T-shaped Thr17 phosphorylated PLB structures are compatible with SERCA. This suggests that the sampled

L- and T-shaped structures, which are the most sampled conformations in phosphorylated states, are structurally different in Ser16 and Thr17 phosphorylated PLB.

4. Discussion

In this paper, the effects of Ser16 and Thr17 phosphorylation on the conformational sampling of PLB were studied and compared with a previous study of PLB in DPPC bilayer by means of the HDGB implicit membrane model [22]. To the best of our knowledge, this work is the first simulation reported for single site phosphorylated PLB at Thr17. This work also covers the conformational sampling of p16-PLB over time scales that are much longer than previously reported simulations of p16-PLB. Previous short explicit simulations did not reach the time scales needed for lipid relaxation or focused only on the CP domain of PLB in water. Using an implicit description of the membrane with the HDGB model allowed us to cover much

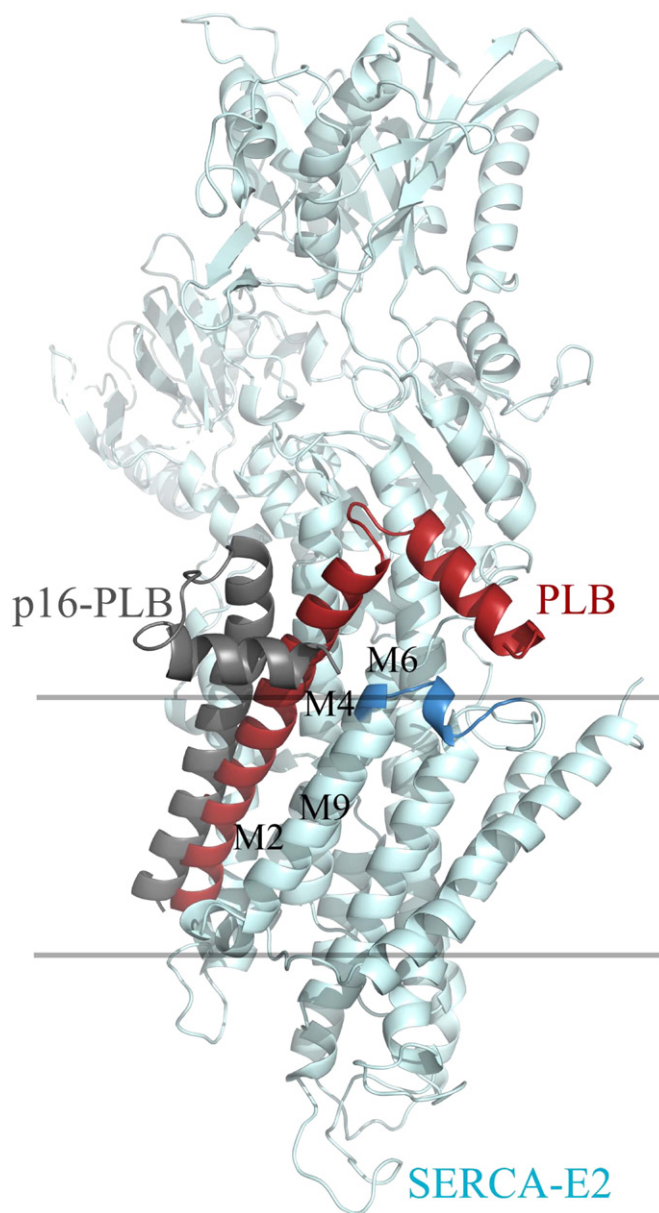


Fig. 7. Manually docked model of PLB and p16-PLB into SERCA in the E2 conformation. PLB and p16-PLB structures correspond to the minima in the PMFs and SERCA structure is from the crystal structure with the PDB entry code of 1IWO. Upper part of the TM helix number M9 of SERCA and a part of the loop connecting helices M8 and M9 are highlighted.

longer time scales with moderate computational resources. Furthermore, the use of replica exchange simulation methodology and averaging over multiple separate simulations further increased the effective time scales much beyond of what could be reached with conventional constant-temperature explicit lipid simulations. We estimate that although our simulations are only on the scale of tens of nanoseconds, the dynamics described here occurs in reality on microsecond to millisecond timescales as a result of the combined acceleration from replica exchange sampling and avoidance of slow lipid relaxation kinetics.

The key finding of the present work is that phosphorylation of PLB at Ser16 significantly affects conformational sampling of PLB in the CP domain in such a way that it increases the chances of a clash with SERCA in the E2 state. Upon phosphorylation at Ser16, the helical content of the C terminus of the CP domain reduces and new conformations with a break in the CP domain are sampled. Also structures with completely buried Tyr6 residue are observed for p16-PLB. These types of conformations are not observed for p17-PLB. Our results suggest that if p16-PLB remains in the same binding site as PLB, the number of clashes between SERCA and PLB increases significantly. To remain bound to SERCA, we therefore hypothesize that p16-PLB changes its interaction site to prevent such clashes. A model constructed from crystal structure of SERCA in the E2 form and one of the most sampled p16-PLB structures in our simulation is shown in Fig. 7. This complex model takes into account available cross-link data for p16-PLB, which is summarized in Table S1 (see Methods section). For comparison, a model constructed with one of the most highly populated structures in our previous simulation of unphosphorylated PLB simulation [22] and SERCA–E2 complex is shown in Fig. 7. The use of the cross-link data introduces uncertainty into the proposed complex model, but while individual cross-links provide only loose restraints, combined data from all available cross-links limit the possibility for alternative conformations. As can be seen, the TM domain of p16-PLB is more detached from SERCA

relative to the TM domain of PLB in order to prevent clashes between the membrane-inserted CP domain of p16-PLB and the loop connecting helices M8 and M9 in SERCA (highlighted in Fig. 7). Such a partial detachment is consistent with the cross-links reported for the lower part of helix M4 in SERCA after PLB phosphorylation at Ser16 [41]. Previous modeling studies of the PLB–SERCA complex have suggested that the TM domain of PLB closely interacts with a groove constructed by helices M2, M4, M6 and M9 of SERCA in the E2 state in the absence of calcium ions thereby preventing SERCA from undergoing a conformational switch to E1 [40]. According to our model, p16-PLB becomes sufficiently detached from this groove to allow the transition from E2 to E1 and subsequently enable enzyme activity [29,34].

The case of p17-PLB appears to involve a different mechanism. According to our results, the conformations sampled for p17-PLB are still largely compatible with the tight complex proposed for unphosphorylated PLB. A possible explanation for how p17-PLB may nevertheless regulate SERCA activity would involve a shift in binding equilibrium towards PLB dissociation upon p17 phosphorylation. The two different proposed mechanisms for Ser16 and Thr17 phosphorylation are illustrated in Fig. 8. We further speculate that Ser16 phosphorylation may be the typical regulatory mechanism for normal cycling of SERCA activity while Thr17 phosphorylation may become involved under special circumstances where complete PLB dissociation is more desirable.

Ser16 phosphorylation alone is sufficient for the maximal cardiac response to β -adrenergic stimulation [11]. However, differential effects have been reported for Thr17 phosphorylation with respect to the frequency dependence during electrical stimulation [8,9], in increased heart cell contractions, in calcium transients of aerobic interval trained mice [12], and during mechanical recovery after stresses like acidosis and stunning [15]. Based on these observations, Thr17 phosphorylation of PLB may play a role when fast changes in the heart rate are needed or when a fast response is required for heart

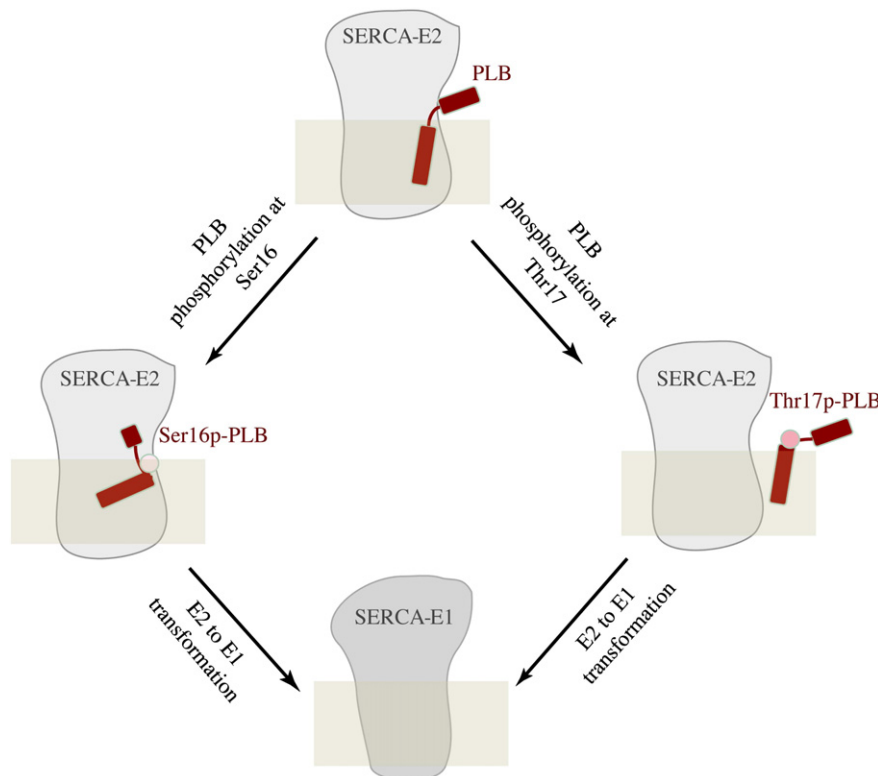


Fig. 8. A hypothetical diagram for the interaction of PLB and SERCA. Phosphorylation of PLB at Ser16 changes the binding site of SERCA and p16-PLB while PLB is still partially bound to SERCA. The p17PLB hypothetically detaches from SERCA. Either phosphorylation pathway induces the E2 to E1 conformational change in SERCA and activates the pump.

functioning such as an electric shock. Complete dissociation of PLB as proposed for p17-PLB may facilitate a more rapid activation of SERCA compared to p16-PLB, which is proposed to remain bound to SERCA. Clearly, further studies are needed to understand these questions more completely. In particular, there is a need for more detailed structural data with respect to PLB–SERCA interactions.

Several *in vivo* studies suggest a sequential nature of phosphorylation [5,64,65] on the two phosphorylation sites and indicate that Thr17 phosphorylation may typically depend on PLB pre-phosphorylation at Ser16 [66]. Furthermore, experimental studies have suggested an additive effect of double-phosphorylation in terms of activating SERCA [13–15]. This raises the questions of how the double-phosphorylation state affects the conformational sampling of PLB compared to the single-phosphorylated PLB variants. Simulations of the double-phosphorylated state are difficult because of significant pK_a shifts expected to result from two neighboring phosphate groups that are likely to partial charge neutralization of one of the phosphates. Because we expect that the pK_a shifts are strongly coupled to conformational changes of PLB, we believe that pH dynamics simulation techniques are needed to adequately study this system. Such simulations are outside the scope of this study but are being considered in future work.

5. Conclusion

Conformational changes introduced by phosphorylation of PLB at Ser16 and Thr17 have been studied through molecular dynamics simulations. Taking advantage of an implicit membrane environment and replica exchange sampling phosphorylated PLB conformations were sampled on estimated microsecond–millisecond timescales. Phosphorylation on either site introduced different changes in the conformational sampling and the resulting energy landscapes. Phosphorylation at Ser16 increases the chances of clash with SERCA and suggests that steric effects cause the reorientation of PLB respect to SERCA. Thr17 phosphorylation, on the other hand, does not seem to increase the number of clashed structures with SERCA significantly. This suggests that instead of reorientation, PLB may dissociate from SERCA after phosphorylation on Thr17. Based on the model we present here Ser16 and Thr17 phosphorylation of PLB appear to have different mechanisms, which may reflect different physiological role of each individual phosphorylation.

Acknowledgments

Access to the High Performance Computer Center at Michigan State University and TeraGrid computer facilities (TG-MCB090003) and financial support from the NSF Grant 0447799 are acknowledged.

Appendix A. Supplementary data

Supplementary data to this article can be found online at <http://dx.doi.org/10.1016/j.bbamem.2012.08.017>.

References

- [1] H.K. Simmerman, L.R. Jones, Phospholamban: protein structure, mechanism of action, and role in cardiac function, *Physiol. Rev.* 78 (1998) 921–947.
- [2] J.M. Autry, L.R. Jones, Functional Co-expression of the canine cardiac Ca²⁺ pump and phospholamban in *Spodoptera frugiperda* (SF21) cells reveals new insights on ATPase regulation, *J. Biol. Chem.* 272 (1997) 15872–15880.
- [3] A.D. Wegener, H.K. Simmerman, J.P. Lindemann, L.R. Jones, Phospholamban phosphorylation in intact ventricles. Phosphorylation of serine 16 and threonine 17 in response to beta-adrenergic stimulation, *J. Biol. Chem.* 264 (1989) 11468–11474.
- [4] J.S. Sham, L.R. Jones, M. Morad, Phospholamban mediates the beta-adrenergic-enhanced Ca²⁺ uptake in mammalian ventricular myocytes, *Am. J. Physiol.* 261 (1991) H1344–H1349.
- [5] M. Kuschel, P. Karczewski, P. Hempel, W.P. Schlegel, E.G. Krause, S. Bartel, Ser16 prevails over Thr17 phospholamban phosphorylation in the beta-adrenergic regulation of cardiac relaxation, *Am. J. Physiol.* 276 (1999) H1625–H1633.
- [6] J.P. Lindemann, A.M. Watanabe, Phosphorylation of phospholamban in intact myocardium. Role of Ca²⁺-calmodulin-dependent mechanisms, *J. Biol. Chem.* 260 (1985) 4516–4525.
- [7] C. Mundina-Weilenmann, L. Vittone, M. Ortale, G.C. de Cingolani, A. Mattiazzi, Immunodetection of phosphorylation sites gives new insights into the mechanisms underlying phospholamban phosphorylation in the intact heart, *J. Biol. Chem.* 271 (1996) 33561–33567.
- [8] D. Hagemann, M. Kuschel, T. Kuramochi, W. Zhu, H. Cheng, R.P. Xiao, Frequency-encoding Thr17 phospholamban phosphorylation is independent of Ser16 phosphorylation in cardiac myocytes, *J. Biol. Chem.* 275 (2000) 22532–22536.
- [9] R.A. Bassani, A. Mattiazzi, D.M. Bers, CaMKII is responsible for activity-dependent acceleration of relaxation in rat ventricular myocytes, *Am. J. Physiol.* 268 (1995) H703–H712.
- [10] D. Hagemann, R.P. Xiao, Dual site phospholamban phosphorylation and its physiological relevance in the heart, *Trends Cardiovasc. Med.* 12 (2002) 51–56.
- [11] G. Chu, J.W. Lester, K.B. Young, W. Luo, J. Zhai, E.G. Kranias, A single site (Ser16) phosphorylation in phospholamban is sufficient in mediating its maximal cardiac responses to beta-agonists, *J. Biol. Chem.* 275 (2000) 38938–38943.
- [12] O.J. Kemi, O. Ellingsen, M. Ceci, S. Grimaldi, G.L. Smith, G. Condorelli, U. Wisloff, Aerobic interval training enhances cardiomyocyte contractility and Ca²⁺ cycling by phosphorylation of CaMKII and Thr-17 of phospholamban, *J. Mol. Cell. Cardiol.* 43 (2007) 354–361.
- [13] L.M. Bilezikjian, E.G. Kranias, J.D. Potter, A. Schwartz, Studies on phosphorylation of canine cardiac sarcoplasmic reticulum by calmodulin-dependent protein kinase, *Circ. Res.* 49 (1981) 1356–1362.
- [14] E.G. Kranias, Regulation of Ca²⁺ transport by cyclic 3',5'-AMP-dependent and calcium-calmodulin-dependent phosphorylation of cardiac sarcoplasmic reticulum, *Biochim. Biophys. Acta* 844 (1985) 193–199.
- [15] A. Mattiazzi, C. Mundina-Weilenmann, C. Guoxiang, L. Vittone, E. Kranias, Role of phospholamban phosphorylation on Thr17 in cardiac physiological and pathological conditions, *Cardiovasc. Res.* 68 (2005) 366–375.
- [16] J. Zamoan, A. Mascioni, D.D. Thomas, G. Veglia, NMR solution structure and topological orientation of monomeric phospholamban in dodecylphosphocholine micelles, *Biophys. J.* 85 (2003) 2589–2598.
- [17] N.J. Traaseth, L. Shi, R. Verardi, D.G. Mullen, G. Barany, G. Veglia, Structure and topology of monomeric phospholamban in lipid membranes determined by a hybrid solution and solid-state NMR approach, *Proc. Natl. Acad. Sci. U. S. A.* 106 (2009) 10165–10170.
- [18] N.J. Traaseth, J.J. Buffly, J. Zamoan, G. Veglia, Structural dynamics and topology of phospholamban in oriented lipid bilayers using multidimensional solid-state NMR, *Biochemistry* 45 (2006) 13827–13834.
- [19] P. Pollesello, A. Annala, M. Ovaska, Structure of the 1–36 amino-terminal fragment of human phospholamban by nuclear magnetic resonance and modeling of the phospholamban pentamer, *Biophys. J.* 76 (1999) 1784–1795.
- [20] C.B. Karim, T.L. Kirby, Z. Zhang, Y. Nesmelov, D.D. Thomas, Phospholamban structural dynamics in lipid bilayers probed by a spin label rigidly coupled to the peptide backbone, *Proc. Natl. Acad. Sci. U. S. A.* 101 (2004) 14437–14442.
- [21] J. Zamoan, F. Nitu, C. Karim, D.D. Thomas, G. Veglia, Mapping the interaction surface of a membrane protein: unveiling the conformational switch of phospholamban in calcium pump regulation, *Proc. Natl. Acad. Sci. U. S. A.* 102 (2005) 4747–4752.
- [22] M. Sayadi, S. Tanizaki, M. Feig, Effect of membrane thickness on conformational sampling of phospholamban from computer simulations, *Biophys. J.* 98 (2010) 805–814.
- [23] Y. Houndonougbo, K. Kuczera, G.S. Jas, Structure and dynamics of phospholamban in solution and in membrane bilayer: computer simulations, *Biochemistry* 44 (2005) 1780–1792.
- [24] M.G. Paterlini, D.D. Thomas, The alpha-helical propensity of the cytoplasmic domain of phospholamban: a molecular dynamics simulation of the effect of phosphorylation and mutation, *Biophys. J.* 88 (2005) 3243–3251.
- [25] Y. Sugita, N. Miyashita, T. Yoda, M. Ikeguchi, C. Toyoshima, Structural changes in the cytoplasmic domain of phospholamban by phosphorylation at Ser16: a molecular dynamics study, *Biochemistry* 45 (2006) 11752–11761.
- [26] T. Kim, J. Lee, W. Im, Molecular dynamics studies on structure and dynamics of phospholamban monomer and pentamer in membranes, *Proteins* 76 (2009) 86–98.
- [27] S. Pantano, E. Carafoli, The role of phosphorylation on the structure and dynamics of phospholamban: a model from molecular simulations, *Proteins Struct. Funct. Bioinform.* 66 (2007) 930–940.
- [28] E.E. Metcalfe, N.J. Traaseth, G. Veglia, Serine 16 phosphorylation induces an order-to-disorder transition in monomeric phospholamban, *Biochemistry* 44 (2005) 4386–4396.
- [29] N.J. Traaseth, D.D. Thomas, G. Veglia, Effects of Ser16 phosphorylation on the allosteric transitions of phospholamban/Ca(2+)-ATPase complex, *J. Mol. Biol.* 358 (2006) 1041–1050.
- [30] R.J. Mortishiresmith, S.M. Pitzenberger, C.J. Burke, C.R. Middaugh, V.M. Garsky, R.G. Johnson, Solution structure of the cytoplasmic domain of phospholamban—phosphorylation leads to a local perturbation in secondary structure, *Biochemistry* 34 (1995) 7603–7613.
- [31] R.J. Mortishires-Smith, H. Broughton, V.M. Garsky, E.J. Mayer, R.G. Johnson, Structural studies on phospholamban and implications for regulation of the Ca²⁺-ATPase, *Annals of the New York Academy of Sciences* 853 (1998) 63–78.
- [32] S.A. Tatulian, L.R. Jones, L.G. Reddy, D.L. Stokes, L.K. Tamm, Secondary structure and orientation of phospholamban reconstituted in supported bilayers from polarized attenuated total reflection FTIR spectroscopy, *Biochemistry* 34 (1995) 4448–4456.

- [33] P. Pollesello, A. Annala, Structure of the 1–36 N-terminal fragment of human phospholamban phosphorylated at Ser-16 and Thr-17, *Biophys. J.* 83 (2002) 484–490.
- [34] J. Li, D.J. Bigelow, T.C. Squier, Phosphorylation by cAMP-dependent protein kinase modulates the structural coupling between the transmembrane and cytosolic domains of phospholamban, *Biochemistry* 42 (2003) 10674–10682.
- [35] M. Li, R.L. Cornea, J.M. Autry, L.R. Jones, D.D. Thomas, Phosphorylation-induced structural change in phospholamban and its mutants, detected by intrinsic fluorescence, *Biochemistry* 37 (1998) 7869–7877.
- [36] M. Asahi, E. McKenna, K. Kurzydowski, M. Tada, D.H. MacLennan, Physical interactions between phospholamban and sarco(endo)plasmic reticulum Ca²⁺-ATPases are dissociated by elevated Ca²⁺, but not by phospholamban phosphorylation, vanadate, or thapsigargin, and are enhanced by ATP, *J. Biol. Chem.* 275 (2000) 15034–15038.
- [37] S. Negash, Q. Yao, H. Sun, J. Li, D.J. Bigelow, T.C. Squier, Phospholamban remains associated with the Ca²⁺- and Mg²⁺-dependent ATPase following phosphorylation by cAMP-dependent protein kinase, *Biochem. J.* 351 (2000) 195–205.
- [38] C.B. Karim, Z. Zhang, E.C. Howard, K.D. Torgersen, D.D. Thomas, Phosphorylation-dependent conformational switch in spin-labeled phospholamban bound to SERCA, *J. Mol. Biol.* 358 (2006) 1032–1040.
- [39] J.P. Glaves, C.A. Trieber, D.K. Ceholski, D.L. Stokes, H.S. Young, Phosphorylation and mutation of phospholamban alter physical interactions with the sarcoplasmic reticulum calcium pump, *J. Mol. Biol.* 405 (2011) 707–723.
- [40] C. Toyoshima, M. Asahi, Y. Sugita, R. Khanna, T. Tsuda, D.H. MacLennan, Modeling of the inhibitory interaction of phospholamban with the Ca²⁺ ATPase, *Proc. Natl. Acad. Sci. U. S. A.* 100 (2003) 467–472.
- [41] Z. Chen, B.L. Akin, L.R. Jones, Mechanism of reversal of phospholamban inhibition of the cardiac Ca²⁺-ATPase by protein kinase A and by anti-phospholamban monoclonal antibody 2D12, *J. Biol. Chem.* 282 (2007) 20968–20976.
- [42] D.D. Thomas, L.G. Reddy, C.B. Karim, M. Li, R. Cornea, J.M. Autry, L.R. Jones, J. Stamm, Direct spectroscopic detection of molecular dynamics and interactions of the calcium pump and phospholamban, in: R.G.K.E.G. Johnson (Ed.), *Cardiac Sarcoplasmic Reticulum Function and Regulation of Contractility*, vol. 853, 1998, pp. 186–194.
- [43] L.T. Chen, Q. Yao, T.A. Soares, T.C. Squier, D.J. Bigelow, Phospholamban modulates the functional coupling between nucleotide domains in Ca-ATPase oligomeric complexes in cardiac sarcoplasmic reticulum, *Biochemistry* 48 (2009) 2411–2421.
- [44] A. Panahi, M. Feig, Conformational sampling of influenza fusion peptide in membrane bilayers as a function of termini and protonation states, *J. Phys. Chem. B* 114 (2010) 1407–1416.
- [45] S. Tanizaki, M. Feig, Molecular dynamics simulations of large integral membrane proteins with an implicit membrane model, *J. Phys. Chem. B* 110 (2006) 548–556.
- [46] Y. Sugita, Y. Okamoto, Replica-exchange molecular dynamics method for protein folding, *Chem. Phys. Lett.* 314 (1999) 141–151.
- [47] A.D. MacKerell, D. Bashford, M. Bellott, R.L. Dunbrack, J.D. Evanseck, M.J. Field, S. Fischer, J. Gao, H. Guo, S. Ha, D. Joseph-McCarthy, L. Kuchnir, K. Kuczera, F.T.K. Lau, C. Mattos, S. Michnick, T. Ngo, D.T. Nguyen, B. Prodhom, W.E. Reiher, B. Roux, M. Schlenkrich, J.C. Smith, R. Stote, J. Straub, M. Watanabe, J. Wiorkiewicz-Kuczera, D. Yin, M. Karplus, All-atom empirical potential for molecular modeling and dynamics studies of proteins, *J. Phys. Chem. B* 102 (1998) 3586–3616.
- [48] A.D. MacKerell Jr., M. Feig, C.L. Brooks III, Improved treatment of the protein backbone in empirical force fields, *J. Am. Chem. Soc.* 126 (2004) 698–699.
- [49] S. Tanizaki, M. Feig, A generalized Born formalism for heterogeneous dielectric environments: application to the implicit modeling of biological membranes, *J. Chem. Phys.* 122 (2005).
- [50] M. Feig, W. Im, C.L. Brooks III, Implicit solvation based on generalized Born theory in different dielectric environments, *J. Chem. Phys.* 120 (2004) 903–911.
- [51] J.P. Ryckaert, G. Ciccotti, H.J.C. Berendsen, Numerical-integration of cartesian equations of motion of a system with constraints—molecular-dynamics of n-alkanes, *J. Comput. Phys.* 23 (1977) 327–341.
- [52] C.L. Brooks, M. Berkowitz, S.A. Adelman, Generalized Langevin Theory for many-body problems in chemical-dynamics—gas-surface collisions, vibrational-energy relaxation in solids, and recombination reactions in liquids, *J. Chem. Phys.* 73 (1980) 4353–4364.
- [53] M. Feig, Kinetics from implicit solvent simulations of biomolecules as a function of viscosity, *J. Chem. Theory Comput.* 3 (2007) 1734–1748.
- [54] J. Chocholousova, M. Feig, Balancing an accurate representation of the molecular surface in generalized born formalisms with integrator stability in molecular dynamics simulations, *J. Comput. Chem.* 27 (2006) 719–729.
- [55] B.R. Brooks, R.E. Bruccoleri, B.D. Olafson, D.J. States, S. Swaminathan, M. Karplus, Charmm—a program for macromolecular energy, minimization, and dynamics calculations, *J. Comput. Chem.* 4 (1983) 187–217.
- [56] M. Feig, J. Karanicolas, C.L. Brooks III, MMTSB Tool Set: enhanced sampling and multiscale modeling methods for applications in structural biology, *J. Mol. Graph. Model.* 22 (2004) 377–395.
- [57] S. Kumar, D. Bouzida, R.H. Swendsen, P.A. Kollman, J.M. Rosenberg, The weighted histogram analysis method for free-energy calculations on biomolecules. 1. The method, *J. Comput. Chem.* 13 (1992) 1011–1021.
- [58] W.L. DeLano, *The PyMOL Molecular Graphics System*, 2002.
- [59] C. Toyoshima, H. Nomura, Structural changes in the calcium pump accompanying the dissociation of calcium, *Nature* 418 (2002) 605–611.
- [60] Z. Chen, D.L. Stokes, L.R. Jones, Role of leucine 31 of phospholamban in structural and functional interactions with the Ca²⁺ pump of cardiac sarcoplasmic reticulum, *J. Biol. Chem.* 280 (2005) 10530–10539.
- [61] Z. Chen, B.L. Akin, D.L. Stokes, L.R. Jones, Cross-linking of C-terminal residues of phospholamban to the Ca²⁺ pump of cardiac sarcoplasmic reticulum to probe spatial and functional interactions within the transmembrane domain, *J. Biol. Chem.* 281 (2006) 14163–14172.
- [62] Z. Chen, D.L. Stokes, W.J. Rice, L.R. Jones, Spatial and dynamic interactions between phospholamban and the canine cardiac Ca²⁺ pump revealed with use of heterobifunctional cross-linking agents, *J. Biol. Chem.* 278 (2003) 48348–48356.
- [63] L.R. Jones, R.L. Cornea, Z. Chen, Close proximity between residue 30 of phospholamban and cysteine 318 of the cardiac Ca²⁺ pump revealed by intermolecular thiol cross-linking, *J. Biol. Chem.* 277 (2002) 28319–28329.
- [64] J.P. Lindemann, L.R. Jones, D.R. Hathaway, B.G. Henry, A.M. Watanabe, beta-Adrenergic stimulation of phospholamban phosphorylation and Ca²⁺-ATPase activity in guinea pig ventricles, *J. Biol. Chem.* 258 (1983) 464–471.
- [65] J.P. Lindemann, Alpha-adrenergic stimulation of sarcolemmal protein phosphorylation and slow responses in intact myocardium, *J. Biol. Chem.* 261 (1986) 4860–4867.
- [66] W. Luo, G. Chu, Y. Sato, Z. Zhou, V.J. Kadambi, E.G. Kranias, Transgenic approaches to define the functional role of dual site phospholamban phosphorylation, *J. Biol. Chem.* 273 (1998) 4734–4739.